

Refractive index sensor based on the natural roughness of a directly fabricated D-shape fiber for biological and environmental monitoring purposes

Sarah Pulikottil Alex^{a,*}, Rafal Kasztelaniec^{b,c}, Grzegorz Stepniewski^c, Andrius Baltuška^a, Ryszard Buczynski^{b,c}, Ignác Bugár^{a,d}

^a Photonics Institute, Vienna University of Technology, Gusshausstrasse 27-29, 1040 Vienna, Austria

^b Faculty of Physics, University of Warsaw, Pasteura 5, 02-093 Warsaw, Poland

^c Łukasiewicz Research Network– Institute of Microelectronics and Photonics, al. Lotników 32/46, 02-668 Warsaw, Poland

^d Institute of Chemistry and Environmental Sciences, University of Ss. Cyril and Methodius, Námestie J. Herdu 577/2, 917 01 Trnava, Slovakia

ARTICLE INFO

Keywords:

Fiber optic sensor
Evanescent wave effect
D-shape fiber

ABSTRACT

We present a novel fiber optics sensor approach using an intentionally designed silica fiber that requires no additional processing after fabrication. The fiber, drawn from a D-shaped preform, maintains a D-shape cross-section along its entire length, ensuring high uniformity of geometrical parameters such as core diameter and the flattened surface distance from the core. The primary advantage of our approach is its unique ability to sense analytes at arbitrary distances from the fiber end and at any interaction length using the evanescent wave effect. We demonstrate the sensing performance by exposing a short fiber section (4 cm) to a liquid analyte in its pure form without using any signal-enhancing interlayer. Importantly, the output signal remains unchanged when water is applied as the medium, while exposure to an alcoholic medium significantly increases transmission. We further analyze the refractive index sensitivity of the technique by varying the water-isopropyl alcohol mixture ratio at a 1030 nm wavelength in a few-mode propagation regime. The results, interpreted in terms of the elimination of Rayleigh scattering losses of the higher-order modes by index matching between the fiber and the sensing medium, underscore the potential of our approach for water contamination sensing in both biological and environmental applications with distributed sensing capability, thereby addressing a critical need in the field.

1. Introduction

Optical fiber sensors (OFS) are widely used in various fields, including industrial, chemical, and biological applications [1,2]. They offer several advantages, such as simplicity of construction, versatility, resistance to electromagnetic interference, chemical neutrality, compact size, lightweight, reliability, and multiplexing capability. OFS measurements include temperature, stress, pressure, and refractive index (RI). In particular, measuring the change in RI offers the possibility of developing a range of label-free biochemical sensors [3]. This leverages the fact that, for example, during a chemical reaction such as antibody-antigen binding or DNA hybridization, the concentration change affects the RI of the solution [4]. In the design of a fiber-optic RI sensor, it is essential that the light propagating through the core effectively interacts

with the external medium, such as by evanescent waves [5]. The interaction of light with the external medium can be achieved in various fiber optic systems. The most important include long-period gratings induced in a fiber core [6,7], fiber tapers [8,9], bend fibers [10], splicing different fibers to obtain interferometric structures [11], photonic crystal fibers (PCF) [12], antiresonant optical fibers [13], and D-shaped fibers [14]. Such fibers can be used directly or in interferometric systems based on Mach Zehnder [15] and Fabry-Perot [16] interferometers. To achieve selectivity in the detection of biological or chemical compounds and to increase the signal of the sensor, the area where the light field interacts with the measured medium is often chemically modified [17] or additionally coated with a thin layer of metal [18] or dielectric [14]. Such an approach results in Surface Plasmon Resonance (SPR) [19] or Lossy Mode Resonance (LMR) [20,21], where the resonance wavelength

* Corresponding author.

E-mail address: sarah.alex@tuwien.ac.at (S. Pulikottil Alex).

<https://doi.org/10.1016/j.yofte.2024.104036>

Received 2 August 2024; Received in revised form 21 October 2024; Accepted 4 November 2024

Available online 11 November 2024

1068-5200/© 2024 The Authors. Published by Elsevier Inc. This is an open access article under the CC BY license (<http://creativecommons.org/licenses/by/4.0/>).

changes with the RI of the tested substance. Table 1 shows the typical resolutions achieved in various fiber optic sensors.

One versatile solution for measuring RI with and without resonances is sensors based on D-shaped optical fiber [14,37]. D-shaped optical fiber is formed from a standard, usually single-mode fiber (SMF), by partially removing the cladding. Various mechanical [38], chemical [39,40], and ablative [41–43] methods are used for this purpose. The problem with these approaches is low accuracy and repeatability because each fiber is processed individually. Since the processing is done on a micrometer scale, the D-shaped fiber sections produced may differ from each other, and therefore their optical properties also vary. As a result, each fiber must be calibrated separately [44]. The method recently proposed by G. Stepniewski et al. [36] for directly fabricating D-shape fiber by drawing a modified preform makes it possible to obtain tens of meters of practically identical fiber. As a result, hundreds of identical sensors are fabricable using this fiber.

To further simplify the sensor's design and make it as low-cost as possible, we investigated the application potential of such a fiber without using any additional technological processes, such as etching or sputtering thin layers. In particular, we will show that a fiber guiding several modes highly depends on the transmission of the refractive index (RI) of the surrounding medium without any spectral effect. It represents an essential novelty of this work, in contrast to most fiber optics sensor approaches and the previous publications dealing with the same type of fiber [36]. We have chosen mixtures of water and isopropyl alcohol as the sensing medium, enabling significant RI changes and ensuring safety. An exciting feature of our approach is the invariance of the output signal in the water medium when the sensing region is surrounded by it. However, a further increase in the RI of the medium greatly eliminates the losses, indicating the role of Rayleigh scattering at the flattened cladding surface. Our concept, namely the selective increase of the transmission of the higher-order modes, is supported by numerical simulations of both the mode structure of the fiber and the RI dependence of their losses. Moreover, the experimental study was extended by monitoring the output beam shape, and these observations confirmed this concept.

2. Novel D-shape fiber and experimental apparatus

The silica-made D-shape fiber described in [36] was used in this work. The basis of this approach is to modify the preform rather than the finished fiber. The preform was cut and ground on one side to decrease the distance of the germanium-doped core to the flattened cladding surface below the core diameter. The diameter of the preform was 20

Table 1

Comparison of the resolution of fiber optic refraction index sensors (Abbreviations used in the table: LPFG – Long Period Fiber Grating, FBG – Fiber Bragg Grating, PCF – Photonics Crystal Fibers, SPR – Surface Plasmon Resonance, LMR – Lossy Mode Resonance).

Basis of sensor operation	Additional feature	Resolution [RIU]	Reference
LPFG	thin film	$1 \times 10^{-3} - 1 \times 10^{-5}$	[6,7,22,23]
	SPR	1×10^{-5}	
FBG		$1 \times 10^{-5} - 1 \times 10^{-7}$	
Tapering		2.5×10^{-5}	[24]
Interferometric		$1 \times 10^{-4} - 1 \times 10^{-6}$	[8,9,25,26]
PCF		$1 \times 10^{-5} - 1 \times 10^{-6}$	[11,27]
Hollow-core		8.5×10^{-5}	[12,28]
SPR		1×10^{-6}	[13]
LMR		$1 \times 10^{-5} - 1 \times 10^{-7}$	[29,30]
D-shape		$1 \times 10^{-5} - 1 \times 10^{-6}$	[31,32]
		$1 \times 10^{-3} - 1 \times 10^{-5}$	[14]
	LPFG	2.7×10^{-5}	[33]
	PCF	1.92×10^{-5}	[34]
	SPR	9.8×10^{-6}	[35]
	LMR	2×10^{-5}	[36]
This article		2×10^{-3}	

mm, which allows for two orders of magnitude higher precision in shaping related to the final fiber geometry compared to the processing of a standard fiber. The preform was then drawn on an optical tower, ensuring a cross-section reduction by a factor of 200. The result is a D-shape fiber with a slightly rounded surface close to the core (Fig. 1). By controlling the drawing process parameters such as temperature, delivery, and fiber drawing rate, the curvature of this surface, the shape of the core, and the distance of the core from the edge of the fiber can be controlled to some extent.

The fiber became slightly rounded, and the side surfaces achieved high smoothness due to the glass's viscosity, elastic forces, and surface tension during the drawing process. Simultaneously, the final roughness also depends on the parameters of the fiber drawing (Fig. 2). For the fiber used in this study, the roughness (Ra) is about 30 nm, and the RMS is less than 40 nm.

The particular eccentric position of the fiber core, preserved along the propagation axis, supports the interaction of the guided field with gaseous or liquid analytes along the arbitrary fiber length. Our recent study used a fiber with the geometrical parameters labeled in Fig. 1, featuring a slightly elliptical core with main axis dimensions of approximately 7 and 8 μm and the flattened surface distance from the core at about 2 μm . The refractive index of the core and cladding is 1.456 and 1.450, respectively, at 1030 nm. Fiber samples with 20–50 cm lengths, protected with standard acrylate coating, were used. The coating on a 4 cm section of all samples in their middle part was removed by immersing the fiber in acetone for about 20 min. Subsequently, the softened coating was stripped step by step by gently applying tiny wooden rods. This removal allowed interaction with the analyte across the thinnest area of the cladding via the evanescent wave effect. Ytterbium-based femtosecond fiber oscillator radiation (100 fs pulses at 1030 nm with a bandwidth of about 15 nm) was launched into one end of the fiber, while the other end was butt-coupled to a multi-mode collection fiber of a high-resolution spectrometer.

The wavelength was chosen to be short enough to operate within the high transmission spectral range of the applied analytes, yet long enough to exhibit the evanescent wave effect beyond the 2 μm flat cladding. For alignment purposes, 633 nm HeNe radiation was also transmitted through the D-shape fiber, which was insensitive to the surrounding medium along the sensing area of the fiber. Another advantageous property of the 1030 nm radiation is its support for few-mode propagation in the fiber, identified as crucial for the demonstrated sensing approach. The femtosecond fiber laser was selected as a source for its operational stability and its broad spectrum, which was advantageous for registering the output field using a spectrometer. Sub-nanojoule pulse energies were applied to prevent any nonlinear interactions. Neither the analyzed water nor the isopropyl alcohol (IPA) medium exhibited significant absorption features in this spectral range. Therefore, the spectral changes were homogeneous across the entire spectral band of the laser used. The intensity changes of the transmitted radiation were recorded under various conditions, not only altering the analyte composition but also the interaction length and sensing geometry. The spatial distribution of the output field was alternatively monitored using an infrared beam profiler, onto which the fiber end facet was imaged. This extension of the registration technique allowed for examining beam shape alterations alongside spectral intensity changes and the relationships between these two output characteristics.

3. Refraction index sensing in straight fiber geometry

The effect of the fiber length surrounded by testing liquid on transmitted spectral intensity was examined first in straight fiber geometry with an overall length of 20 cm. Spectral registration applying IPA along 1 cm, 2 cm, and 4 cm of the sensing region is depicted in Fig. 3a, showing monotonic transmission enhancement at each step. As mentioned, both the distilled water and isopropyl alcohol show negligible absorption in the bandwidth of the transmitted spectra. The noisy character of the

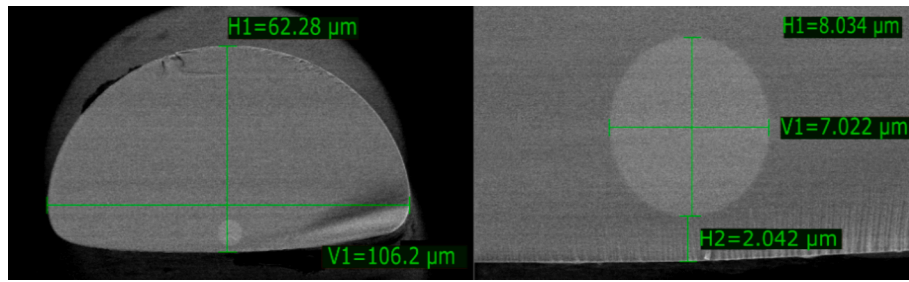


Fig. 1. Scanning electron microscope image of the cross-section of the used D-shape fiber. The same geometry is maintained along the entire length of fiber.

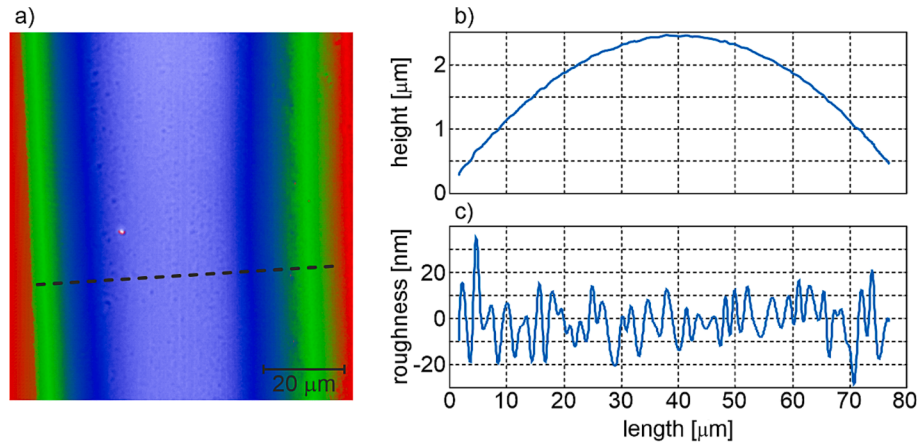


Fig. 2. Fiber surface investigated on a white light interferometer: a) image of the surface, b) cross-section in the transverse direction, c) roughness after removal of surface roundness.

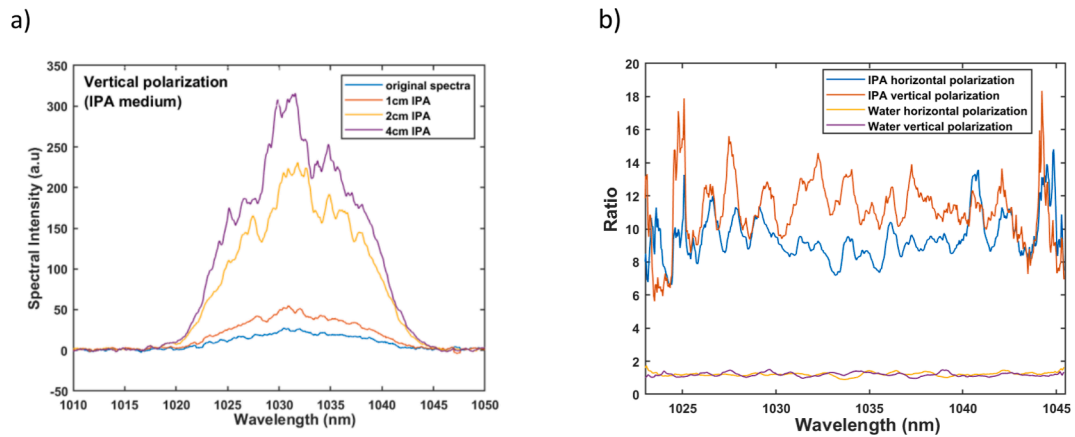


Fig. 3. (a) Output spectra registered under vertical polarization in the case of 20 cm fiber with straight geometry under increasing length of sensing region surrounded by IPA (b) Spectral intensity ratios under complete surrounding of the sensing region by the liquid vs. without it for both main polarization directions.

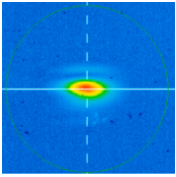
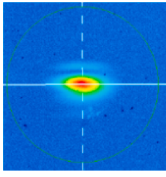
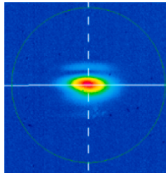
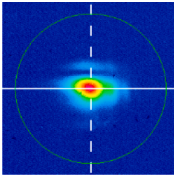
spectra is caused by the multimode interference effect of both the sensing and spectra-collecting fibers. Similar registrations also applied water as a testing liquid, resulting in negligible transmission changes. To better compare the output spectra under different experimental conditions, ratio curves were constructed by dividing it with the reference spectra registered under the same conditions, but without applying any analyte (original spectra). Fig. 3b compares these spectral ratios under the complete surrounding of the sensing region by the liquid in the cases of IPA and water for the two main polarization directions. The observations reveal that only IPA affects the transmission, increasing the output intensity by a factor of around 10. Meanwhile, water has no effect, which is represented by a ratio near 1. Furthermore, vertical polarization, meaning field orientation perpendicular to the flattened

cladding of the fiber, causes higher spectral intensity ratios exceeding 10 in the central area of the laser bandwidth. Thus, both the refractive index of the liquid medium and the polarization direction of the guided radiation influence the output spectral intensity. The original spectra were integrated along the spectral bandwidth to quantitatively evaluate the spectral results, eliminating the interference effect. Information about the transmitted optical power under various experimental conditions was acquired in this way.

Besides spectral registration, the shape of the output beam was studied experimentally by increasing the fiber length surrounded by pure IPA. Sequential enhancement of the interaction length from 1 cm to 4 cm resulted in a monotonic reduction of the output beam's ellipticity, accompanied by the transmission enhancement presented in Table 2.

Table 2

Near-field camera images, length of the sensing region, camera integration time and beam ellipticity expressing mutual reduction of the output beam ellipticity and improvement of the intensity with the increasing length of the sensing region.

Beam Profile				
Sensing medium	Only air	1 cm IPA	2 cm IPA	4 cm IPA
Integration time	398.1 ms	398.1 ms	290.4 ms	225.4 ms
Ellipticity	0.36	0.45	0.49	0.73

Due to the increasing output intensity the camera integration time was sequentially reduced to avoid saturation effect. The ellipticity was calculated as the simple ratio of the beam diameters along the Y and X axes at half intensity. This observation indicates a higher transmission enhancement rate of transversal modes, which are structured perpendicular to the flattened fiber cladding surface when the analyte has a higher RI than water. This statement is based on findings from repeated experiments using water, which did not cause any observable change in the transmitted beam shape with increasing length of the sensing region. Thus, the invariance of the water medium on the transmitted optical field was observed in both spectral and camera registration approaches.

The significant increase in transmission (more than one order of magnitude for vertical polarization) when using IPA instead of water indicates the potential for concentration measurements of these miscible liquids. Therefore, our next experimental series focused on investigating volume fraction sensitivity, considering the refractive indices of IPA and distilled water to be 1.370 and 1.327 at 1030 nm, respectively. Fig. 4a presents the output spectra obtained by applying the analyte along a 4 cm sensing region in straight fiber geometry with an increasing IPA volume ratio in 10 % increments. This study allows for quantitative analysis of the IPA effect because controlling the volume ratio using micropipettes is more precise than sequentially increasing the surrounded fiber length by dropping the analyte. The results were processed by calculating the individual spectra's integral spectral intensity and the mixture's refractive index with varying IPA content based on the Arago-Biot formula [45]. The dependence of integral intensity on the refractive index is presented in Fig. 4b. A monotonic increase in output intensity with increasing IPA concentration was observed, with a linear relationship indicating a refractive index sensitivity below 0.002. Considering the linear fit parameters, this dependence corresponds to a multiplication of transmitted intensity by a factor of 150 for a refractive index change of 1 RIU from the 1.327 level representing the water RI. All experiments revealed higher sensitivity for vertical polarization

orientation. Therefore, only these results are presented. The obtained RI sensitivity is relatively low compared to other methods (Table 1). However, it was achieved for an unmodified fiber, without additional layers to increase sensitivity and resolution, and using only light intensity measurements and not more expensive systems like a spectrometer or interrogator.

The beam shape at the output fiber facet was also monitored during this measurement series, and we identified the same trend as observed with varying surrounding fiber lengths. However, the increasing influence of IPA on the sensing region was now ensured by its increasing concentration, resulting in enhanced beam circularity and peak intensity. The alteration of the IPA volume ratio f_{IPA} study confirmed that the water medium does not change the output field characteristics, as f_{IPA} enhancement had a similar effect to the increasing length of the surrounding fiber sensing region. Both the comparison of the effects of water and IPA medium (Fig. 3b) and the increasing IPA measure studies indicate that our system is invariant when exchanging the surrounding air with water and vice versa. Thus, our sensing approach appears to be a promising tool for water contamination monitoring, yielding signals only when the analyte's refractive index is higher than the water RI.

4. Analysis of results

A numerical analysis of the guiding properties of the studied D-shaped fiber was performed to clarify the obtained experimental results. A finite difference eigenmode solver (Lumerical) was used for the modal analysis, considering air as the surrounding medium. The cross-sectional geometry of the D-shaped fiber, in accordance with the SEM image in Fig. 1, was considered with a simplified, completely flat cladding surface, as its curvature is negligible near the fiber core. The refractive index values of the core and cladding were calculated using the Sellmeier equation related to pure silica and germanium-doped silica glass with a 6 % doping level. The number of guided modes in the fiber were

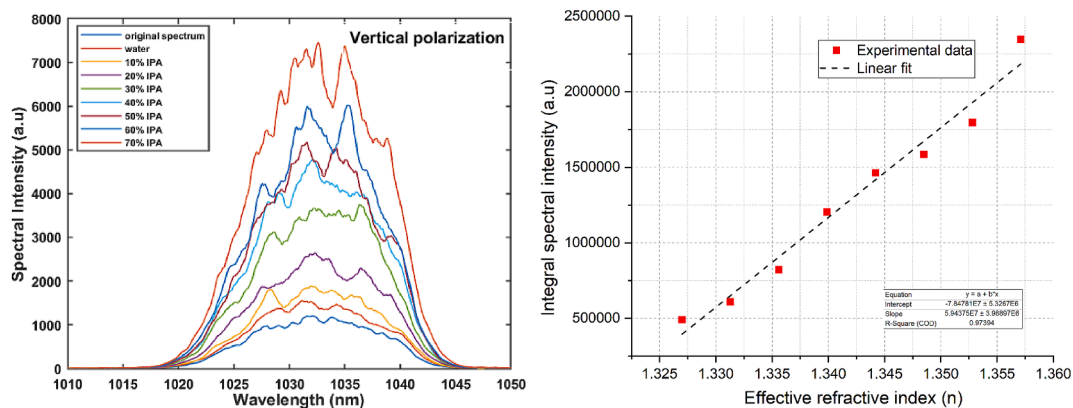


Fig. 4. (a) Transmitted spectral dependence on isopropanol volume ratio in water under vertical polarization orientation. (b) Dependence of output integral intensity on the refractive index of the mixture.

identified as six at 1030 nm, including both orthogonal polarization directions of the three types of modes shown in Fig. 5 as LP₀₁, LP_{11x}, and LP_{11y}. The losses of the individual modes were also analyzed, revealing their sequential increase with the highest losses in the case of LP_{11y} structured toward the flattened surface. Moreover, the opposite effect of increasing the refractive index of the medium was predicted, showing enhancement of losses for LP_{11x} and their reduction for LP_{11y} for both polarization directions. Thus, the elimination of losses in the most lossy mode, LP_{11y}, is expected with increasing IPA effect at the sensing region, accompanied by simultaneous loss enhancement of the LP_{11x} mode. Therefore, one can expect the beam shape to become more circular as the losses between the two higher-order modes with orthogonal structures become more balanced. This corresponds to our experimental results showing beam ellipticity with a longer axis parallel to the flattened surface and its reduction under increasing IPA effect.

The weak point of this interpretation is the extremely low calculated losses, at the level of 10^{-5} dB/cm, which cannot account for the significant changes observed in transmission and beam shape. Therefore, we measured the losses of both the original D-shape fiber sample with acrylate coating and after its removal, resulting in a significant increase in losses in the latter case. This observation confirms the crucial role of the surrounding medium at the flattened surface in affecting fiber transmission properties. Next, the roughness of the flattened surface was analyzed using a white light interferometer (Veeco), revealing the most frequent values between 10–80 nm and an RMS around 40 nm. These results highlight the role of Rayleigh scattering at the cladding surface, impacting the evanescent field of the individual guided modes to varying degrees. It can be inferred that Rayleigh scattering has a greater effect on higher-order modes because their evanescent field penetration depth is larger than that of the fundamental mode. Thus, the losses of the higher-order modes are more affected by the cladding roughness through the Rayleigh scattering effect. Consequently, we expect significantly higher losses than those predicted under the assumption of an ideally smooth cladding surface in numerical simulations.

The intensity of the scattered light, which is the primary source of the additional losses, depends on the refractive index difference between the guiding medium and the scattering objects. Standard acrylate coatings match the silica refractive index, significantly reducing scattering losses. In contrast, when the coating is removed, the index contrast of the air-silica interface causes significant losses, as observed. We measured a decrease in transmitted power by a factor of about 20 in an identical D-shape fiber with a length of 20 cm when the coating was removed along a 4 cm distance. According to the Rayleigh scattering formula, one can expect a sequential elimination of scattered intensity by increasing the refractive index of the surrounding medium, as performed in the IPA-

water mixture experiment. Therefore, we interpret the observed significant transmission changes by the reduced losses of the LP_{11y} mode with increasing RI of the surrounding medium, a trend strengthened by the Rayleigh scattering phenomenon.

Correspondingly, the increasing losses of the LP_{11x} mode with rising refractive index are also influenced by scattering but in the opposite direction. The increase in refractive index eliminates the scattering effect, making the dependence of LP_{11x} mode losses on the medium RI significantly weaker than that of the LP_{11y} mode. Additionally, losses calculated for the LP_{11x} mode were an order of magnitude lower ($1.062 \cdot 10^{-5}$ vs. $9.055 \cdot 10^{-5}$ dB/cm), rendering these changes negligible compared to the dominant effect of reducing LP_{11y} mode losses. The simplified geometric aspect of our interpretation is depicted in Fig. 6, illustrating the dominant scattering effect on the LP_{11y} mode and beam shape change due to its elimination, considering the superposition principle of the transversal modes.

5. Conclusions

We propose an innovative approach for refractive index sensing of liquid analytes using D-shape fiber, including performance analysis and interpretation of the main findings. The fiber was fabricated using a novel method based on a D-shaped preform, allowing the drawing of D-shape fiber with a uniform cross-section along its entire length. This fiber component enables its application as a sensor at arbitrary positions along the propagation axis, supporting distributed sensing performance. To preserve this advantageous feature, the sensing was demonstrated using the fiber in its pure form, without any modification by additional layers or surface functionalization. To determine the sensitivity of the D-shape sensor, the protective coating was removed over a distance of several centimeters. This removal results in reduced transmission, which is recovered by applying an analyte with a sufficient index of refraction. Our findings indicate that the output signal does not change in the case of a water medium, while exposure to an alcoholic medium significantly increases the transmission. Furthermore, the refractive index sensitivity of the technique was analyzed at 1030 nm wavelength by exposing the fiber to a water-isopropanol mixture, changing the mixing ratio in a few-mode propagation regime. We registered about 10 dB linear enhancement of the output intensity with an increase in the RI of the medium from 1.327 to 1.370, which allows RI sensitivity at the level of 0.002. The observed trend would result in a 150-fold increase of the transmitted intensity, assuming the same linear dependence under refraction index enhancement by 1 RIU. Further sensitivity improvement is possible by enhancing the registration part of the apparatus, eliminating multimode interference of the spectral collecting fiber, and stabilizing

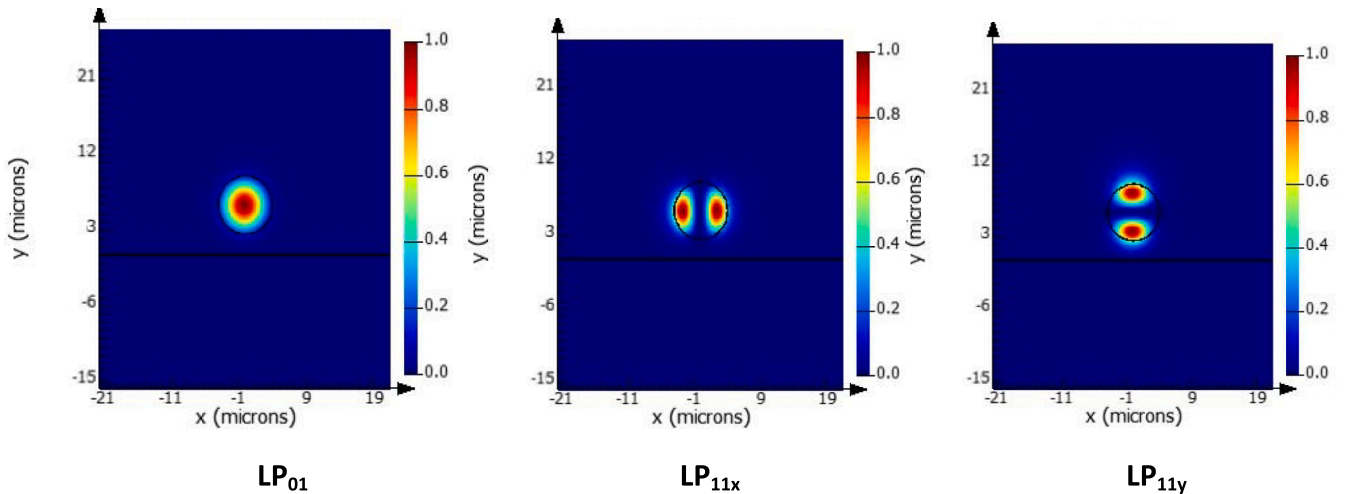


Fig. 5. Simulated profiles of different transversal guided modes of the D-shape fiber exposed by air at the flattened cladding surface at 1030 nm.

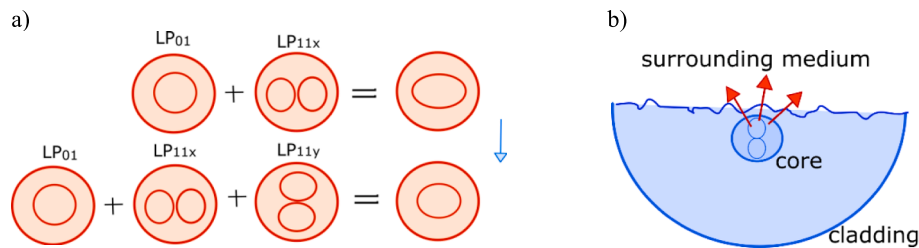


Fig. 6. (a) Superposition effect of modes ensemble with an asymmetric cladding geometry and after its elimination (b) LP_{11y} mode experiences higher scattering losses in comparison to other modes.

the sensing part of the fiber. The fiber experienced small geometrical changes during the repeated surrounding and drying processes when the samples with different water-IPA volume ratios were tested. These precautions can potentially improve RI sensitivity by one order of magnitude.

It is important to stress that the main results of this work, namely the water invariance and the 10 dB transmission increase under IPA exposure, were repeated several times using different fiber pieces with the same geometry. Therefore, the presented approach has commercialization potential after eliminating the mentioned drawbacks. Most similar works demonstrate sensing performance regarding boundary or resonant wavelength shift; in contrast, our method requires only intensity registration instead of spectral registration. However, such fiber optics sensing requires stabilization of all parts of the system and intensity calibration under the actual system parameters. On the other hand, the calibration of most sensing systems is necessary before commercial application, and the studied fiber has proven that the magnitude of the sensing signal is preserved using fiber from the same drawing series. Another advantageous aspect of the presented fiber is that kilometer-range length is available with similar parameters. Thus one polishing process enables the realization of hundreds of sensing apparatuses. Compared to the traditional D-shaped fiber sensing approach, it supports lower production costs, as it is necessary to perform fiber polishing for all individual systems in those cases. Moreover, an advantageous feature of the proposed approach is that signal enhancement was observed only when the RI increased above the water level, expressing linear dependence. Therefore, this cost-effective sensing technique could be applied to different species in water solutions when it causes an increase of the refractive index. Such a sensing approach has many potential applications for the analysis of water solutions with biological and environmental significance.

CRedit authorship contribution statement

Sarah Pulikottil Alex: Writing – original draft, Visualization, Methodology, Investigation, Formal analysis. **Rafal Kasztelan:** Writing – review & editing, Visualization, Software, Investigation, Formal analysis. **Grzegorz Stepniewski:** Visualization, Validation, Resources, Conceptualization. **Andrius Baltuška:** Supervision, Resources, Project administration. **Ryszard Buczynski:** Supervision, Resources, Project administration. **Ignác Bugár:** Writing – review & editing, Supervision, Project administration, Methodology, Conceptualization.

Declaration of competing interest

The authors declare that they have no known competing financial interests or personal relationships that could have appeared to influence the work reported in this paper.

Funding sources

This work was supported by Austrian Science Fund (projects I 5453-N), National Science Center, Poland (projects TECHMATSTRATEG-III/

0042/2019–00, CEUS-UNISONO 2020/02/Y/ST7/00136).

Data availability

Data will be made available on request.

References

- [1] I. Del Villar, I. R. Matias, Optical Fibre Sensors: Fundamentals for Development of Optimized Devices, The Institute of Electrical and Electronics Engineers, Inc. Wiley-IEEE Press, 2021. DOI: <https://doi.org/10.1002/9781119534730.fmatter>.
- [2] Ran Z, He X, Rao Y, Sun D, Qin X, Zeng D, Chu W, Li X, Wei Y., "Fiber-Optic Microstructure Sensors: A Review," *Photonics Sensors*, 11(2), 227–261 (2021). DOI: <https://doi.org/10.1007/s13320-021-0632-7>.
- [3] A. Bekmurzayeva, M. Nurlankyzy, A. Abdossova, Z. Myrkyhyyeva, D. Tosi, All-fiber label-free optical fiber biosensors: from modern technologies to current applications, *Biomed. Opt. Express* 15 (2024) 1453–1473, <https://doi.org/10.1364/BOE.515563>.
- [4] J. Homola, Surface plasmon resonance sensors for detection of chemical and biological species, *Chem. Rev.* 108 (2) (2008) 462–493, <https://doi.org/10.1021/cr068107d>.
- [5] S. Pissadakis, Lab-in-a-fiber sensors: A review, *Microelectron. Eng.* 217 (2019) 111105, <https://doi.org/10.1016/j.mee.2019.111105>.
- [6] J. Cai, Y. Liu, X. Shu, Long-Period Fiber Grating Sensors for Chemical and Biomedical Applications, *Sensors* 23 (2023) 542, <https://doi.org/10.3390/s23010542>.
- [7] M. Piętrzyńska, M. Dominik, K. Kosiel, M. Janczuk-Richter, K. Szot-Karpińska, E. Brzozowska, L. Shao, J. Niedziółka-Jonsson, W.J. Bock, M. Śmietana, Ultrasensitive tantalum oxide nano-coated long-period gratings for detection of various biological targets, *Biosens. Bioelectron.* 133 (2019) 8–15.
- [8] S. Korposh, S.W. James, S.W. Lee, R.P. Tatam, Tapered Optical Fibre Sensors: Current Trends and Future Perspectives, *Sensors* 9 (2019) 2294, <https://doi.org/10.3390/s19102294>.
- [9] E. Ujah, M. Lai, G. Slaughter, Ultrasensitive tapered optical fiber refractive index glucose sensor, *Sci Rep* 13 (2023) 4495, <https://doi.org/10.1038/s41598-023-31127-4>.
- [10] T. Takeo, H. Hattori, Optical Fiber Sensor for Measuring Refractive Index, *Jpn. J. Appl. Phys.* 21 (1982) 1509, <https://doi.org/10.1143/JJAP.21.1509>.
- [11] M. Śmietana, D. Brabant, W.J. Bock, P. Mikulic, T. Eftimov, Refractive-index Sensing with Inline Core-cladding Intermodal Interferometer Based on Silicon Nitride Nano-coated Photonic Crystal Fiber, *J. Lightwave Techn.* 30 (8) (2012) 1185–1189.
- [12] Q. Liu, Z. Ma, Q. Wu, W. Wang, The biochemical sensor based on liquid-core photonic crystal fiber filled with gold, silver and aluminum, *Opt. Laser Technol.* 30 (2020) 106363, <https://doi.org/10.1016/j.optlastec.2020.106363>.
- [13] X. Cui, J. Li, S. Li, H. Guo, R. Wang, X. Ma, O. Chen, C. Wang, X. Meng, C. Wang, H. Zhang, Y. Zhao, X. Li, G. Li, High Resolution and Sensitivity Negative Curvature Hollow Core Fiber Refractive Index Sensor Based on LSPR, *Plasmonics* 18 (2023) 2375–2383, <https://doi.org/10.1007/s11468-023-01935-5>.
- [14] Y. Ying, G.Y. Si, F.J. Luan, K. Xu, Y.W. Qi, H.N. Li, Recent research progress of optical fiber sensors based on D-shaped structure, *Opt. Laser Technol.* 90 (2017) 149–157, <https://doi.org/10.1016/j.optlastec.2016.11.021>.
- [15] H. Yu, L. Xiong, Z. Chen, Q. Li, X. Yi, Y. Ding, F. Wang, H. Lv, Y. Ding, Ultracompact and high sensitive refractive index sensor based on Mach-Zehnder interferometer, *Opt. Lasers Eng.* 56 (2014) 50–53, <https://doi.org/10.1016/j.optlaseng.2013.12.006>.
- [16] R. Gao, Y. Jiang, W. Diang, Z. Wang, D. Liu, Filmed extrinsic Fabry-Perot interferometric sensors for the measurement of arbitrary refractive index of liquid, *Sens. Actuators B* 177 (2013) 924–928, <https://doi.org/10.1016/j.snb.2012.11.083>.
- [17] S.K. Shukla, C.S. Kushwaha, T. Guner, M.M. Demir, Chemically modified optical fibers in advanced technology: An overview, *Opt. Laser Technol.* 115 (2019) 404–432, <https://doi.org/10.1016/j.optlastec.2019.02.025>.
- [18] F. Chiavaioli, P. Zubiato, I. Del Villar, C.R. Zamarreno, A. Giannetti, S. Tombelli, C. Trono, F.J. Arregui, I.R. Matias, F. Baldini, Femtomolar detection by nanocoated fiber label-free biosensors, *ACS Sens.* 3 (2018) 936–943, <https://doi.org/10.1021/acssensors.7b00918>.

- [19] M. Piliarik, J. Homola, Surface plasmon resonance (SPR) sensors: approaching their limits? *Opt. Express* 17 (2009) 16505–16517, <https://doi.org/10.1364/OE.17.016505>.
- [20] F. Yang, J.R. Sambles, Determination of the optical permittivity and thickness of absorbing films using long-range modes, *J. Mod. Opt.* 44 (1997) 1155–1164, <https://doi.org/10.1080/09500349708230726>.
- [21] F. Chiavaioli, D. Janner, Fiber Optic Sensing With Lossy Mode Resonances: Applications and Perspectives, *J. Lightwave Technol.* 39 (12) (2021) 3855–3870, <https://doi.org/10.1109/JLT.2021.3052137>.
- [22] G.A. Rego, Review of refractometric sensors based on long period fibre gratings, *Sci. World J.* 913418 (2013).
- [23] J. Villatoro, D. Monzón-Hernández, D. Talavera, High resolution refractive index sensing with cladded multimode tapered optical fibre, *Electron. Lett.* 40 (2004) 106, <https://doi.org/10.1049/el:20040069>.
- [24] D. Grobnić, S.J. Mihailov, H. Ding, C.W. Smelser, Bragg grating evanescent field sensor made in biconical tapered fiber with femtosecond IR radiation, *IEEE Photonics Technol. Lett.* 18 (2006) 160–162, <https://doi.org/10.1109/LPT.2005.860372>.
- [25] S. Korposh, S.W. James, S.W. Lee, R.P. Tatam, Tapered Optical Fibre Sensors: Current Trends and Future Perspectives, *Sensors* 19 (2019) 2294, <https://doi.org/10.3390/s19102294>.
- [26] F. Ari, H. Şerbetçi, I. Navruz, Tapered fiber optic refractive index sensor using speckle pattern imaging, *Opt. Fib. Technol.* 79 (2023) 103366, <https://doi.org/10.2139/ssrn.4427681>.
- [27] T. Allsop, F. Floreani, K.P. Jedrzejewski, P.V.S. Marques, R. Romero, D.J. Webb, I. Bennion, Spectral characteristics of tapered LPG device as a sensing element for refractive index and temperature, *J. Lightwave Technol.* 24 (2006) 870–878, <https://doi.org/10.1109/JLT.2005.862426>.
- [28] F. Shi, Y. Wu, J. Wang, L. Zhao, H. Shi, S-tapered photonic crystal fiber interferometers for refractive index sensing, *Opt. Eng.* 52 (2013) 035004.
- [29] Q. Wang, D. Zhang, Y. Qian, X. Yin, L. Wang, S. Zhang, Y. Wang, Research on Fiber Optic Surface Plasmon Resonance Biosensors: A Review, *Photonic Sens.* 14 (2024) 240201.
- [30] B.A. Prabowo, A. Purwidyantri, K.C. Liu, Surface Plasmon Resonance Optical Sensor: A Review on Light Source Technology, *Biosensors (basel)*. 8 (3) (2018) 80, <https://doi.org/10.3390/bios8030080>.
- [31] W. Qi, Z. Wan-Ming, A comprehensive review of lossy mode resonance-based fiber optic sensors, *Opt. Laser in Engineering* 100 (2018) 47–60, <https://doi.org/10.1016/j.optlaseng.2017.07.009>.
- [32] S.K. Vikas, A.K. Mishra, P. Mishra, R.K. Saccomandi, Verma, “Recent Advances in Lossy Mode Resonance-Based Fiber Optic Sensors: A Review”, *Micromachines* 13 (2022) 1921.
- [33] J.N. Dash, R. Jha, On the performance of graphene-based D-shaped photonic crystal fibre biosensor using surface plasmon resonance, *Plasmonics* 10 (5) (2015) 1123–1131, <https://doi.org/10.1007/s11468-015-9912-7>.
- [34] J.N. Dash, R. Jha, Highly sensitive D shaped PCF sensor based on SPR for near IR, *Opt. Quantum Electron.* 48 (2) (2016) 137, <https://doi.org/10.1007/s11082-016-0423-3>.
- [35] D.F. Santos, A. Guerreiro, J.M. Baptista, SPR microstructured D-type optical fiber sensor configuration for refractive index measurement, *IEEE Sens. J.* 15 (10) (2015) 5472–5477, <https://doi.org/10.1109/JSEN.2015.2442335>.
- [36] G. Stepniowski, A. Filipkowski, D. Pysz, J. Warszewski, R. Buczyński, M. Śmietana, R. Kasztelan, From D-shaped to D-shape optical fiber – A universal solution for sensing and biosensing applications, *Measurement* 222 (2023) 113642, <https://doi.org/10.1016/j.measurement.2023.113642>.
- [37] G. Liu, D. Feng, Evanescent wave analysis and experimental realization of refractive index sensor based on D-shaped plastic optical fiber, *Optik* 127 (2) (2016) 690–693, <https://doi.org/10.1016/j.jpleo.2015.10.129>.
- [38] S.M. Tseng, C.L. Chen, Side-polished fibers, *Appl. Opt.* 31 (18) (1992) 3438–3447, <https://doi.org/10.1364/AO.31.003438>.
- [39] L. Yin, M.J. Yan, Z.G. Han, H.L. Wang, H. Shen, R.H. Zhu, High power cladding light stripper using segmented corrosion method: theoretical and experimental studies, *Opt. Express* 25 (8) (2017) 8760–8776, <https://doi.org/10.1364/OE.25.008760>.
- [40] M. Śmietana, M. Koba, P. Mikulic, W.J. Bock, Towards refractive index sensitivity of long-period gratings at level of tens of μm per refractive index unit: fiber cladding etching and nano-coating deposition, *Opt. Express* 24 (11) (2016) 11897–11904, <https://doi.org/10.1364/OE.24.011897>.
- [41] C. Hu, X. Ma, C. Wang, S. Zhou, H. Wu, K. Sun, High-quality rapid fabrication method of a D-shaped optical fiber based on a CO₂ laser, *Opt. Mater. Express* 11 (2021) 2025–2036, <https://doi.org/10.1364/OME.428792>.
- [42] T. Gabler, M. Janik, C. Liao, A. Mysliwiec, M. Koba, M. Jönsson-Niedziółka, Y. Wang, M. Śmietana, Investigation of liquids with microcavity in-line Mach-Zehnder interferometers – impact of the microcavity shape on the sensing performance, *Opt. Fiber Technology* 73 (2022) 103059, <https://doi.org/10.1016/j.yofte.2022.103059>.
- [43] L. Jiang, L. Zhao, S. Wang, J. Yang, H. Xiao, Femtosecond laser fabricated all-optical fiber sensors with ultrahigh refractive index sensitivity: modeling and experiment, *Opt. Express* 19 (18) (2011) 17591, <https://doi.org/10.1364/OE.19.017591>.
- [44] H.H. Qazi, A. Mohammad, H. Ahmad, M.Z. Zulkifli, D-Shaped Polarization Maintaining Fiber Sensor for Strain and Temperature Monitoring, *Sensors* 16 (2016) 1505, <https://doi.org/10.3390/s16091505>.
- [45] J.V. Srinivasu, K. Narendra, K. Shobha Rani, B. Subba Rao, “Refractive index studies of binary liquid mixtures containing 1, 4-butanediol + o-cresol/m-cresol/p-cresol,” *Journal of Chemical and Pharmaceutical Sciences* 11, 261 (2018). DOI: <https://doi.org/10.30558/jchps.20181104003>.